Received: 28 March 2023 | Revised: 3 July 2023 | Accepted: 5 July 2023

DOI: 10.1111/jace.19331

Journal of the American Ceramic Society

RESEARCH ARTICLE

Effect of thermal depolarization on the poling-induced domain texture and piezoelectric properties in Mg-doped NBT-6BT

Laura Cangini | **Andreas Wohninsland** | **Daniel Bremecker** | **Lovro Fulanović** | **Changhao Zhao** | **Jürgen Rödel**

Division of Nonmetallic-Inorganic Materials, Department of Materials and Earth Sciences, Technical University of Darmstadt, Darmstadt, Germany

Correspondence
Laura Cangini, Division of Nonmetallic-Inorganic Materials, Department of Materials and Earth Sciences, Technical University of Darmstadt, 64287 Darmstadt, Germany.
Email: cangini@ceramics.tu-darmstadt.de

Present address
Changhao Zhao, State Key Laboratory of Electrical Insulation and Power Equipment, Xi'an Jiaotong University, Xi'an, Shaanxi, China

Funding information
Wuzhen Laboratory; Deutsche Forschungsgemeinschaft, Grant/Award Number: 414311761

Abstract

Recently, poled $Na_{0.50}Bi_{0.50}TiO_3$-$BaTiO_3$ (NBT-BT)-based polycrystalline materials have been characterized as possessing a high degree of poling-induced domain texture in their remanent state. This finding is suggested to be the reason for their stable mechanical quality factor at high-vibration velocity, making them promising candidates for high-power applications. The materials in consideration are prone to self-heating and thermal run-away, particularly at slightly elevated temperatures. Therefore, this paper evaluates the temperature dependence of the poling-induced domain texture of $(Na_{0.47}Bi_{0.47}Ba_{0.06})TiO_3$ (NBT-6BT) doped with 0.5 mol% of Mg as compared to undoped NBT-6BT. Its influence on small-signal, large-signal, and high-power properties was investigated. To obtain a fundamental understanding of crystal structure, *in-situ* synchrotron measurements were conducted as function of temperature to establish a relationship between structure and piezoelectric properties of both Mg-doped and undoped NBT-6BT materials.

KEYWORDS
hardness, high-power application, piezoelectric materials/properties, polarization, texture

1 | INTRODUCTION

Textured ceramics are aggregates of crystals with a preferred crystallographic orientation[1] and, therefore, a significant degree of anisotropy. They represent a compromise between the highest textured but expensive single crystals and the cheaper but randomly oriented polycrystalline ceramics.

Texture can be induced through forming processes by reorienting the polycrystalline grains along the direction that maximizes their piezoelectric response.[2–4] In this case, the word texturing is referred to as "grain texturing."[5] Alternatively, texture could be induced in the domain structure, so in subregions of grains by, for example, domain engineering techniques. In this latter case, it is referred to as "domain texturing,"[6–8] and it is the type of texturing being referred to by the authors of this study.

Recently, poled NBT-BT-based polycrystalline materials have been discovered to exhibit a high degree of domain texture in their remanent state, even if their structure was

not previously textured using a conventional process.[9] In this case, the electric poling was sufficient to align the ferroelectric domains to a degree of texture almost close to the theoretical maximum achievable, conferring them such a high stability that even an extreme driving force (e.g., high vibration velocity) cannot result in further domain wall movement, hence increasing extrinsic losses.

The authors have attributed this remarkable domain stability to the hardening mechanism of the NBT materials that has been hypothesized to differ from the commonly accepted for lead zirconate titanate (PZT) ones,[10,11] whose degree of domain texture is considerably lower,[6,12,13] and which may be connected to the relaxor nature of NBT materials. They have furthermore suggested that the hardening effect may occur during the electrical poling process and not after it. A similarly high degree of domain texture was also reported in the ferroelectric $0.55Bi(Ni_{1/2}Ti_{1/2})O_3$-$0.45PbTiO_3$ (BNT-45PT) composition.[14] However, the raw diffraction data do not exhibit such a high degree of domain texture, and the texturing factor was calculated in different fashion as compared to our approach, making a comparison difficult.

If, on one hand, the origin of such a high degree of domain texture in NBT-BT-based materials needs more studies for complete understanding, on the other hand, the enhanced texturing rationalizes the high stability of their quality factors when tested at room temperature in high-vibration mode, making them promising candidates for high-power applications.[9,15,16] Because of the high poling-induced domain texture, the strain in NBT-BT-based materials is primarily due to lattice extension and not domain wall motion, whose limited contribution guarantees low losses and high-domain stability of these materials.

Hard-type ferroelectric ceramics are used in a wide range of high-power applications in the industrial, medical, and automotive sectors. Typical examples are ultrasonic motors, transducers, and high-intensity focused ultrasound devices that allow diagnosis and therapy.[17,18] To achieve high output power, these materials must satisfy some requirements, such as reaching high-vibration velocity without degrading their piezoelectric properties and possessing high and stable mechanical quality factors. In addition, they have to show the stability of their piezoelectric properties in a broad operating temperature range to avoid, for example, their thermal depolarization.[19,20] Furthermore, self-heating is an aspect that must be limited as much as possible because it causes a reduced maximum usable vibration velocity.[21,22] It was demonstrated that piezoelectric materials are affected by dielectric, elastic, and piezoelectric losses, and the heat generation at the resonance frequency, where typically piezoelectric ceramics are driven to obtain their maximum displacement, mainly originated from the elastic ones,[23] whereas heat generation at off-resonance is mainly attributed to dielectric losses.[24–26] Due to the importance of the temperature influence, many researchers have focused on investigating the thermal behavior of the electromechanical properties of several systems and how to improve them.[27–31] It turns out that a comprehensive investigation is necessary to understand if poling-induced domain texture is an effective and novel approach for both increasing the hardness in NBT-BT-based ceramics and simultaneously guaranteeing the stability of the piezoelectric properties in an extensive range of temperatures.

In this paper, we therefore evaluate the temperature dependence of the poling-induced domain texture of NBT-6BT doped with 0.5 mol% of Mg in contrast to undoped NBT-6BT. We report on temperature-dependent synchrotron x-ray diffraction measurements, and correlate the structure with the macroscopic properties of the materials quantified with small and large signals, with special focus on high-power conditions.

2 | EXPERIMENTAL

$(Na_{0.47}Bi_{0.47}Ba_{0.06})TiO_3$ and $(Na_{0.47}Bi_{0.47}Ba_{0.06})(Ti_{0.995}Mg_{0.005})O_3$ ceramics, abbreviated hereafter NBT-6BT and NBT-6BT-0.5Mg, respectively, were prepared by solid-state synthesis. Na_2CO_3 (99.5%), Bi_2O_3 (99.975%), $BaCO_3$ (99.8%), TiO_2 (99.6%), and MgO (99.99%), all supplied by Alfa Aesar, were used as raw materials. After a drying treatment at 100°C for 24 h, the starting powders were weighed in their stoichiometric amounts. Then, the NBT-6BT powders were milled in ethanol for 24 h using zirconia-stabilized yttria balls of 3 mm in diameter, whereas the NBT-6BT-0.5Mg powders were milled for 6 h using zirconia-stabilized yttria balls of 10 mm in diameter. The obtained slurries were filtered and dried overnight to eliminate any ethanol residuals. Subsequently, the powders were calcined in alumina crucibles at 900°C for 3 h. As-calcined powders were milled a second time with the same conditions as the first milling, and then pressed into disk-shaped pellets under a uniaxial pressure of 40 MPa. NBT-6BT pellets were sintered at 1150°C for 3 h in an alumina crucible with a heating and cooling rate of 5 K/min, whereas NBT-6BT-0.5Mg pellets were sintered at 1100°C. In both cases, pellets were embedded in a powder of the same composition to avoid the volatilization of elements. As-sintered samples were ground and annealed for 30 min at 400°C to eliminate any residual mechanical stresses induced by grinding.

Samples for synchrotron and high-power measurements were obtained following the same procedure as described above, but utilizing a bar shape of $5 \times 3 \times 1$ mm^3 and $15 \times 3 \times 1$ mm^3, respectively.

Poling was performed in a silicone oil bath at 30°C by applying a DC field of 6 kV/mm for 15 min.

Temperature-dependent synchrotron X-ray diffraction analysis of undoped and doped samples at poled state were carried out at the beamline P02.1 of Deutsches Elektronen-Synchrotron (DESY) with an incident beam energy of 59.80904 keV (error 0.00158), which corresponds to a wavelength of 0.20730 Å (error 0.00001). The high energy of the incident beam enables to penetrate ceramic samples, and ensures that the collected structural information stems from the bulk interior. An area detector (Dectris Pilatus3 X CdTe 2M) was used for studying the orientation-dependent domain texture. The two-dimensional (2D) diffraction patterns were collected at a temperature range from 30°C to 160°C, with 10°C steps.

The 2D patterns were divided into 10 sectors with an angular range of 20° for each sector. The scattering vector (**Q**) of each sector was roughly α degrees from the poling direction (denoted by α sector hereafter), where α ranges from 0° to 90°. One-dimensional patterns were converted from the 2D patterns by integrating the intensity in each azimuth sector using Fit2D.

To obtain a 1D pattern that circumvents the effects of domain texture and is suitable for Rietveld refinement, the angle-dependent 1D patterns were summed up with a geometrically necessary weighting factor according to Equation (1):[32]

$$\langle I\rangle = \sum_{\alpha=0^\circ}^{90^\circ} I(\alpha)\left[\cos(\alpha_i) - \cos(\alpha_j)\right] \quad (1)$$

where $I(\alpha)$ represents the intensity of the α = sector, and α_i and α_j represent the lower and upper angular boundaries of the corresponding sector. The weighted patterns were refined using the Rietveld method and Topas V5 software.

The {111} and {200} reflections of the patterns from different azimuthal sectors are fitted with three peaks with pseudo-Voigt profile function, using the software LIPRAS.[33] The individual peaks are assigned to the tetragonal and rhombohedral phases according to the position relationship obtained from Rietveld refinement. The f_{hkl} parameters, which represent the ratio between the fraction of *hkl*-oriented domains (hereafter, the term "*hkl*-oriented" denotes the orientation where the crystallographic <*hkl*> direction is parallel to the poling direction) at the current state and that at the virgin state were calculated for the tetragonal and rhombohedral phases using Equations (2) and (3) as follows[34]:

$$f_{111} = 4 \times \frac{\frac{I_{111}}{I'_{111}}}{\frac{I_{111}}{I'_{111}} + 3\frac{I_{11\bar{1}}}{I'_{11\bar{1}}}} \quad (2)$$

$$f_{002} = 3 \times \frac{\frac{I_{002}}{I'_{002}}}{\frac{I_{002}}{I'_{002}} + 2\frac{I_{200}}{I'_{200}}} \quad (3)$$

where f_{111} and f_{002} were calculated using the reflections from the rhombohedral phase and tetragonal phase, respectively. I_{hkl} and I'_{hkl} represent the integrated intensity of the hkl reflection at the current state and the reference state, respectively, obtained similar to the texture-free reference patterns following Equation (1).

The direct piezoelectric constants (d_{33}) were quantified 24 h after the poling process, according to European standard[35] using a Berlincourt d_{33}-meter (PiezoMeter System PM 300, Piezotest Pte Ltd.) at 110 Hz.

The thermally stimulated depolarization current (TSDC) measurements were performed by placing the poled samples into a furnace, heating to 200°C at a rate of 2 K/min. The currents were acquired with a Keithley 6485 picoammeter.

The converse temperature-dependent piezoelectric coefficient d_{33} was determined by applying an AC voltage signal of 10 Vpp amplitude at 1 kHz to the specimens, and detecting the sample's displacement by a laser vibrometer (OFV-505 sensor and VDD-E-600 front-end, Polytec GmbH). This measurement was performed from room temperature to 150°C with a 2 K/min heating rate.

Dielectric permittivity was quantified as function of temperature by applying 1 V_{RMS} over a frequency range of 100 Hz to 1 MHz using an LCR meter (HP 4284A). The samples were heated from room temperature up to 450°C, with a heating rate of 2 K/min.

The current density measurements were performed from 25°C to 125°C using an aixPES piezoelectric evaluation system (aixACCT Systems) by applying a triangular signal voltage at 1 Hz. At the same time, the electrically induced mechanical displacement was recorded with a laser interferometer, and the strain of samples was consequently calculated and plotted as function of electric field.

A customized setup with burst excitation was employed to assess the high-power properties at room temperature. For the detailed setup description, please refer to the study by Slabki et al.[36]

For temperature-dependent high-power measurements, the samples were connected to the previously mentioned setup inside the furnace and were accomplished from 20°C to 120°C. At room temperature, three samples of each composition were evaluated, each three times in resonance and antiresonance mode to obtain averaged data points.

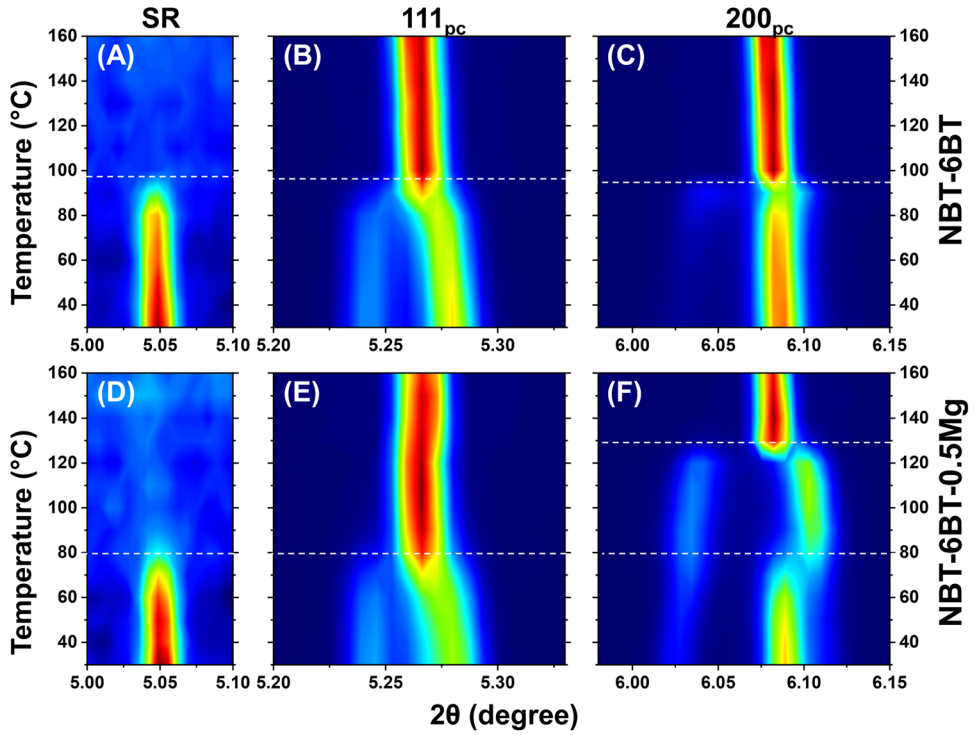

FIGURE 1 Temperature-dependent intensity evolution (colors, arbitrary units) of the superlattice reflection and the $\{111\}_{PC}$ and $\{200\}_{PC}$ reflections of poled NBT-6BT (A–C) and NBT-6BT-0.5Mg (D–F). Displayed is the data integrated over all scattering angles (0°-90°).

The measurements at elevated temperatures were performed on one sample for each composition, which was quantified three times in resonance and antiresonance mode at each temperature step.

3 | RESULTS AND DISCUSSION

3.1 | Crystal structure

The evolution of the $\{111\}_{PC}$ reflection, $\{200\}_{PC}$ reflection, and the superlattice reflection (SR) from *R*3*c* phase as a function of temperature is depicted in Figure 1, with all the patterns integrated from 0° to 90°.

The synchrotron XRD data exhibit peak splitting in the $\{111\}_{PC}$ and $\{200\}_{PC}$ reflections for both poled samples, NBT-6BT and NBT-6BT-0.5Mg. A superlattice reflection (SR) at the 2θ of approximately 5.05° at 30°C (Figure 1) is also noted. This indicates a phase coexistence of rhombohedral *R*3*c* and tetragonal *P*4*mm* phases, as reported in literature,[31,37–39] with the SR caused by the anti-phase octahedral tilting of the *R*3*c* phase. Upon heating, the SR in pure NBT-6BT disappears together with the splitting of the $\{111\}_{PC}$ and $\{200\}_{PC}$ reflections between 90°C and 100°C (Figure 1A–C). This corresponds to the transition into a (pseudo-)cubic structure and correlates with the material's ferroelectric-to-relaxor phase transition ($T_{F\text{-}R}$) and, therefore, depolarization temperature (T_d). The very faint intensity of the 002_T reflection, at around 2θ of 6.03°, increases with increasing temperature between 80°C and 90°C. In contrast, the intensity of the $\{111\}_R$ reflection decreases, implying an increase in tetragonal phase fraction before the actual depolarization occurs, which is consistent with earlier reports.[40] Two regions, therefore, characterize the NBT-6BT system: one up to approximately 100°C where the system reveals a coexistence of the rhombohedral and tetragonal phases, and one above 100°C where the system exhibits a cubic structure.

In contrast, the doped system presents three regimes: the first one, up to 80°C, in which the rhombohedral and tetragonal phases are both present; the second region from 80°C to 130°C in which the tetragonal phase is the predominant one, and the last region above 130°C where the system is cubic. In particular, in NBT-6BT-0.5Mg, the intensity increase of the reflections related to the tetragonal phase already starts between 60°C and 70°C and is more pronounced than in the undoped system, while the SR vanishes at about 90°C. Furthermore, the splitting in the $\{200\}_{PC}$ reflections vanishes at higher temperatures as compared to the undoped material, at around 130°C, which correlates to the increase in T_d upon Mg-doping.[41] This suggests that doping with Mg stabilizes the tetragonal phase on the cost of the rhombohedral phase.

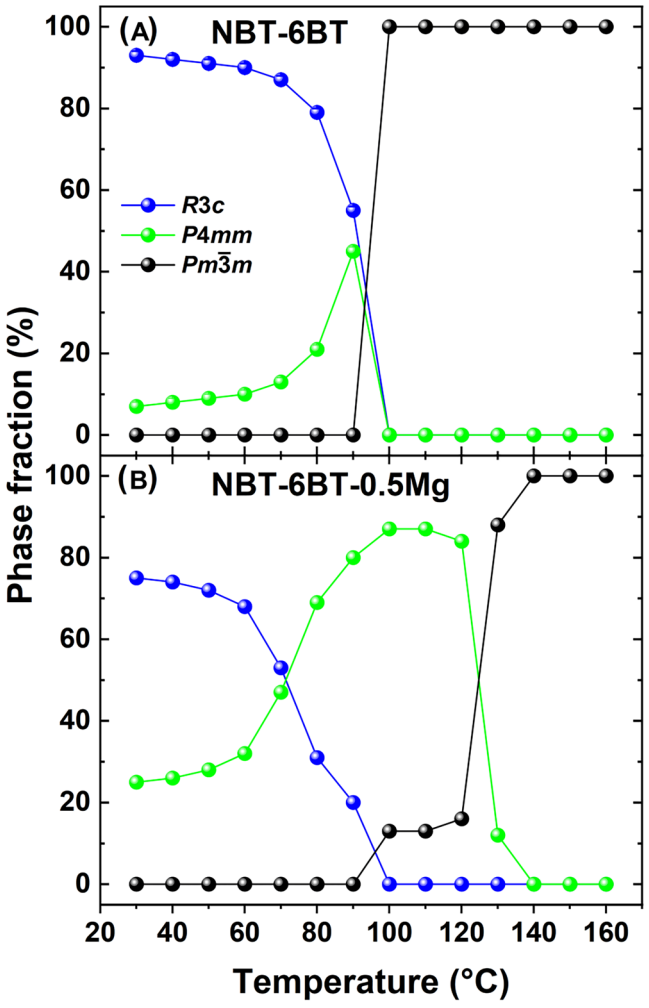

FIGURE 2 Temperature-dependent rhombohedral (*R3c*), tetragonal (*P4mm*), and cubic (*Pm3̄m*) phase fractions of NBT-6BT and NBT-6BT-0.5Mg established from Rietveld refinements.

The phase fractions obtained from full pattern Rietveld refinement, depicted in Figure 2, confirm the qualitatively described changes upon heating based on the inspection of the temperature-dependent peak intensities (Figure 1). The rhombohedral phase fraction in NBT-6BT slightly decreases with increasing temperature until 70°C, then a strong decrease occurs. At 90°C, the rhombohedral phase fraction drops to 55%, while the tetragonal phase fraction increases to 45% (Figure 2A), followed by a rapid ferroelectric-to-relaxor transition at 100°C, above which both the *R3c* and the *P4mm* phases vanish entirely.

In NBT-6BT-0.5Mg, a considerable decrease of the *R3c* phase fraction starts at lower temperatures than pure NBT-6BT (Figure 2B). It decreases to 31% at 80°C, 20% at 90°C, and disappears at 100°C. However, the *P4mm* phase fraction at 30°C in the doped material is higher than in the undoped system, and it strongly increases to 87% at 100°C–110°C before decreasing to 12% at 130°C and vanishing at 140°C.

It is worth noting that the temperature range in which the ferroelectric-to-relaxor transition occurs in pure NBT-6BT-0.5Mg is significantly more extended as compared to the undoped system. The rhombohedral phase, in fact, gradually transforms into the tetragonal phase before becoming cubic.

The evolution of both domain textures of the rhombohedral and tetragonal phases with temperature is depicted in Figure 3. The f_{111} (rhombohedral phase) of NBT-6BT-0.5Mg for the 80° and 90° sectors could not be established, as the 111_R reflection vanishes at high azimuthal angles within the detection limit of the XRD experiment. The f_{111} and the f_{002} (tetragonal phase) of the NBT-6BT system are close to the theoretical upper limits of four and three multiples of the random distribution (MRD), respectively, at low azimuthal angles. This is highly unusual and has been related to the relaxor structure of NBT-6BT.[9] In this work,[9] NBT-6BT and NBT-6BT doped with Zn have been described as having a much higher and stable domain texture than soft PZT, $BaTiO_3$, and $(Ka,Na)NbO_3$, all quantified at room temperature. The established values of f_{111} (Figure 3A) are consistently high for all temperatures considered. In contrast, the degree of texture in the tetragonal phase (Figure 3B), given as f_{002}, is constant for all temperatures except for 90°C up to an azimuth angle of 30°. At 90°C at low azimuthal angles, which is close to the $T_{F\text{-}R}$ of the system, the domain texture is strongly reduced. A decrease in poling-induced texture upon heating is reflected in the change in f_{002} at high azimuthal angles, above 40°.

In NBT-6BT-0.5Mg, the texture of rhombohedral domains (Figure 3C) is even higher than in NBT-6BT and of similar magnitude in the tetragonal case (Figure 3D) for the case of low azimuth degrees. The rhombohedral domain texture is, at first, not affected by the increase in temperature, persists up to 90°C, and then disappears. On the other hand, the domain texture of the tetragonal phase starts decreasing from 70°C, and stabilizes between 90°C and 110°C. The temperature-dependent phase fraction of NBT-6BT-0.5Mg displayed in Figure 2B and the evolution of its rhombohedral and tetragonal domain texture displayed in Figure 3C,D can be directly correlated. The rhombohedral to tetragonal phase transition of the doped system, which occurs at approximately 70°C, is reflected by a decrease of the tetragonal texture in Figure 3D. Thus, it can be inferred that the highly textured rhombohedral phase transforms into untextured tetragonal phase.

Figure S1 provides examples of weighted and refined diffraction patterns of NBT-6BT and NBT-6BT-0.5Mg recorded at 30°C. Close to room temperature, both materials were refined with a two-phase model consisting of

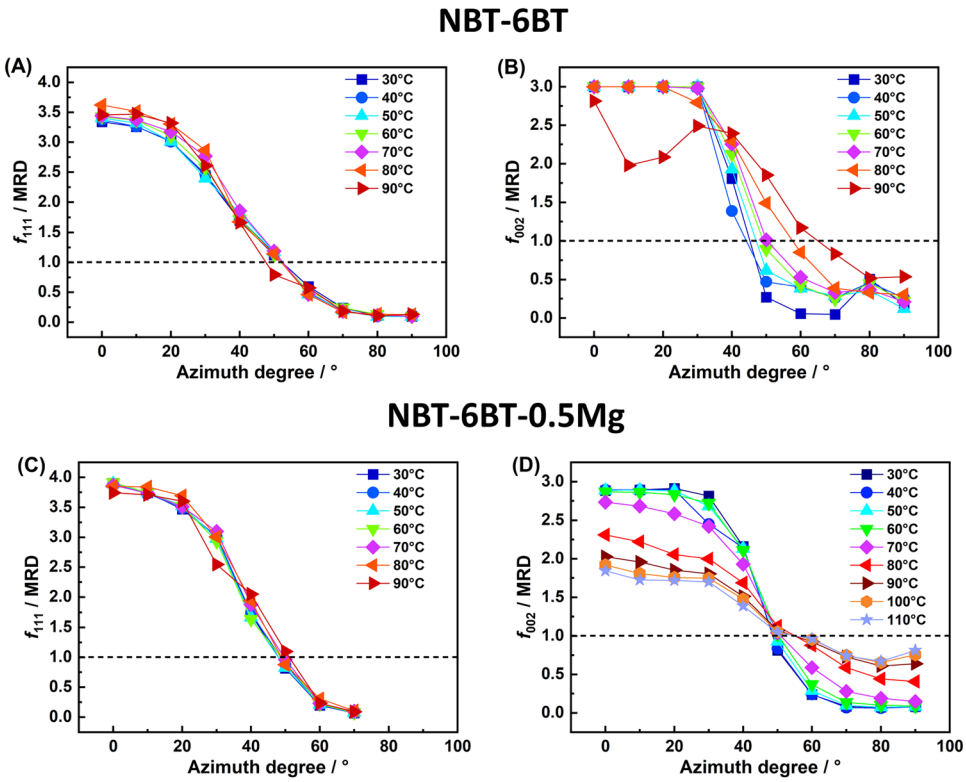

FIGURE 3 Domain texture of the rhombohedral and tetragonal phase in (A and B) NBT-6BT and (C and D) NBT-6BT-0.5Mg at different temperatures.

*R*3*c* and *P*4*mm* phases,[31,38] whereas to refine the data collected at elevated temperatures where the materials exhibit characteristics of cubic symmetry, a cubic $Pm\bar{3}m$ phase was introduced.

Structural parameters established from Rietveld refinements can be found in Tables S1 and S2.

Upon doping, the lattice distortion of the poled material is enhanced in the *R*3*c* and the *P*4*mm* phases at all the temperatures where these phases are present. These observations have been reported before for unpoled Zn- and Mg-doped NBT-BT together with an increase in tetragonal phase fraction.[9,41,42] Also in this study, Mg doping increases the tetragonal phase fraction in the poled state of the bulk material from 7% to 25% at 30°C (Figure 2).

3.2 | Temperature dependence of the small-signal properties

NBT-based ceramics present degradation of their piezoelectric properties at the depolarization temperature (T_d).[43] The T_d can be experimentally detected by performing the TSDC measurement and observing the temperature at which the largest current density peak occurs.

The TSDC results of poled NBT-6BT and NBT-6BT-0.5Mg ceramics are plotted in Figure 4.

In pure NBT-6BT, a sharp current density peak at about 100°C is evident. This temperature represents T_d of the system.[44–46] On the other hand, the current density profile of NBT-6BT-0.5Mg presents a relatively small and broad peak around 85°C, and a sharper and higher one at 140°C. Whereas the latter represents its T_d, which can be correlated to the disappearance of the tetragonal phase, as revealed by synchrotron measurements (Figures 1F and 2), the smaller peak denotes the beginning of the depolarization process, which can be related to the disappearance of the rhombohedral phase of the system at lower temperatures (Figures 1E and 2).

A beginning of thermally induced depolarization at around 85°C was already observed in ZnO composites and Zn^{2+}-doped NBT-BT systems in previous studies.[47] It was rationalized as the shift of the ferroelectric-to-relaxor transition temperature of the tetragonal phase. This was demonstrated to be sharp upon heating unlike the smeared rhombohedral ferroelectric-to-relaxor transition over a broader temperature range.[48] In the case of doped composition, a further rise of current density at temperatures higher than T_d was detected. A tentative explanation for such a behavior is related to the mobile charge defects, most probably oxygen vacancies, which are expected to prevail in higher concentrations than in undoped NBT-6BT.[49,50] The degradation of the piezoelectric properties of

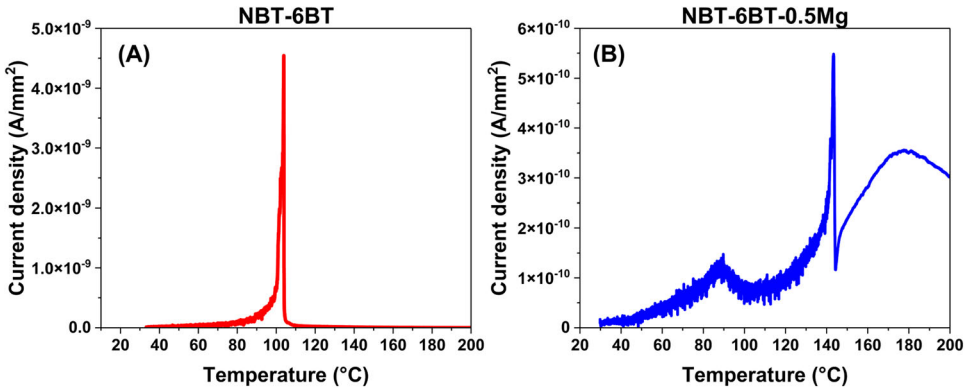

FIGURE 4 Thermally stimulated depolarization current (TSDC) curves of poled NBT-6BT (A) and NBT-6BT-0.5Mg samples (B).

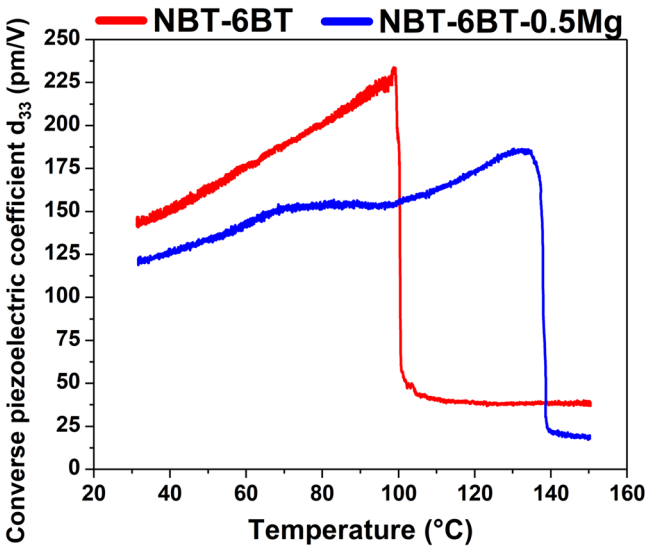

FIGURE 5 Temperature-dependent converse piezoelectric coefficient of NBT-6BT-0.5Mg (blue line) and NBT-6BT (red line).

NBT-6BT and NBT-6BT-0.5Mg at 104°C and 140°C, respectively, is also evidenced by the abrupt drop of the converse piezoelectric coefficients (d_{33}) at the same temperatures (Figure 5).

The converse d_{33} at room temperature in both materials (122 pC/N for NBT-6BT-0.5Mg, and 145 pC/N for NBT-6BT) agrees very well with the direct piezoelectric coefficient obtained with the Berlincourt method (118 ± 2 pC/N for NBT-6BT-0.5Mg, and 145 ± 1 pC/N for NBT-6BT). The d_{33} of the pure NBT-6BT increases until 104°C without any evident anomalies and then drops; in comparison, the piezoelectric coefficient in the NBT-6BT-0.5Mg features a plateau from about 70°C to 90°C before the rise ensues again. This temperature regime is, therefore, confirmed to be critical for the doped system and is in good agreement with synchrotron measurements, which demonstrate the gradual disappearance of the rhombohedral phase.

It is worth noting that in none of the materials of this study, complete disappearance of the d_{33} occurred at the T_d, consistent with results of other studies that reveal that polarization can extend over a large temperature range into the ergodic state in relaxors, as well as above T_c in ferroelectrics.[51,52] The dielectric responses of poled NBT-BT and NBT-6BT-0.5Mg samples as a function of the temperature are depicted in Figure 6.

Frequency dispersion is absent for poled NBT-6BT up to 104°C, the temperature at which the T_{F-R} occurs in NBT-6BT.[53] In contrast, the anomaly (marked by the blue arrow), which appears at around 85°C in the Mg-doped sample, could be attributed to the structural change of the system when it starts de-texturing and the rhombohedral phase vanishes.

Above the respective T_{F-R}, both systems exhibit a relaxor state, with permittivity strongly depending on frequency. The permittivity of doped material at low frequencies increases much faster than those of high frequencies, leading presumably to the Maxwell–Wagner effect as it plays an essential role in contributing to the permittivity of the doped system.[54]

Above 144°C, free charges may be activated near the interfaces in the material and migrate under the influence of the applied electric field. Consequently, the dielectric permittivity undergoes a variation, resulting in an increased value.

3.3 | Temperature dependence of large-signal properties

The remanent polarization of poled NBT-6BT and NBT-6BT-0.5Mg samples was calculated as the mean of the positive remanent polarization (P_{r+}) and the negative remanent polarization (P_{r-}). In analogy, the coercive electric field of the materials is taken as the mean of the positive remanent coercive field (E_{c+}) and

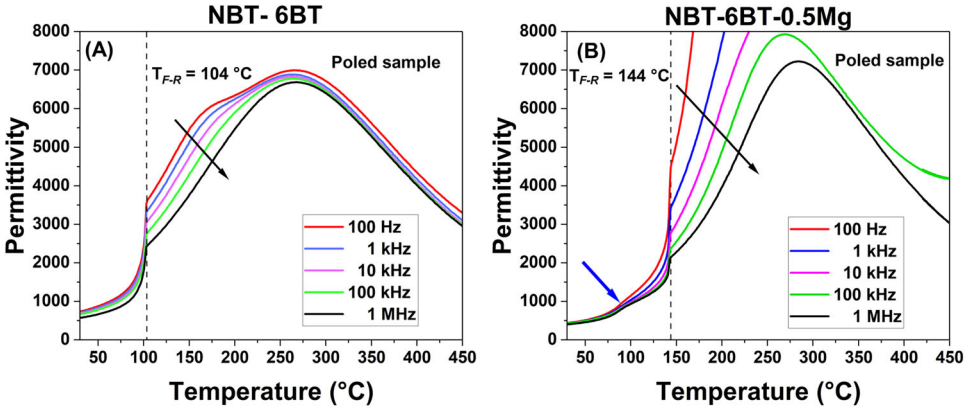

FIGURE 6 Temperature-dependent dielectric permittivity of NBT-6BT (A) and NBT-6BT-0.5Mg (B).

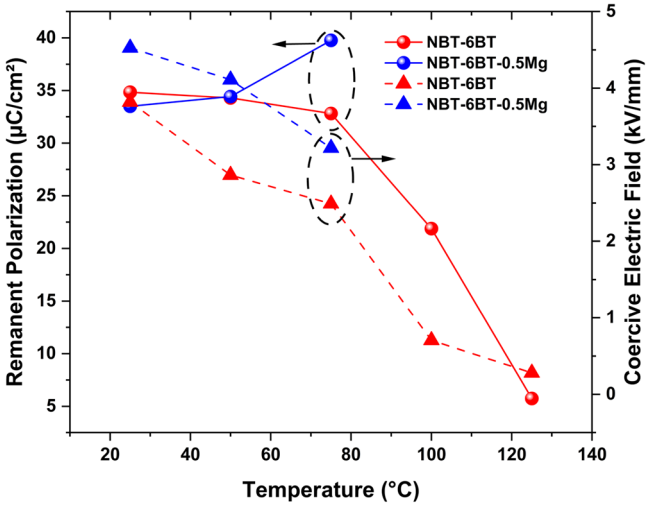

FIGURE 7 Remanent polarization and coercive electric field of poled NBT-6BT and NBT-6BT-0.5Mg samples as function of temperature (the polarization of NBT-6BT-0.5Mg above 75°C was not accessible due to leaky behavior).

the negative remanent coercive field (E_{c-}). The values, extracted from the polarization hysteresis loops reported in Figure S2, are depicted in Figure 7 as function of temperature.

NBT-6BT and NBT-6BT-0.5Mg samples feature comparable remanent polarization at 25°C. Furthermore, in pure NBT-6BT, the remanent polarization is almost constant up to 75°C, and significantly decreases only above this temperature. In contrast, the Mg-doped samples reveal little back-switching with the result that the remanent polarization exhibits a small increase. At higher temperature, the conductivity is increased to the point that meaningful polarization loops cannot be determined anymore. An explanation is probably the enhanced mobility of oxygen vacancies at these moderate temperatures,[55] which are additionally accelerated at high electric fields.[56] The doped material displays a coercive field of around 1 kV/mm higher than the undoped one. This again, like the reduced back-switching, typically accompanies hardening behavior.

From the polarization (P-E) and strain (S-E) hysteresis loops depicted in Figure S2, it is clear that at 100°C NBT-6BT displays an ergodic relaxor behavior denoted by a slim P-E loop and absence of negative strain. In contrast, the negative strain in NBT-6BT-0.5Mg samples is present in all temperatures tested as its ferroelectric-to-relaxor transition temperature (140°C) has not been reached yet.

NBT-6BT-0.5Mg features square-like P-E loops, particularly at 25°C. Moreover, the domain switching occurs over a very narrow electric field range, whereas P-E loops of the NBT-6BT appear slanted, meaning that similar polarization change occurs over a larger electric field range. Consequently, for the two materials, the same amount of charge flows during switching, but in the Mg-doped system, it happens in a smaller field interval than in NBT-6BT, producing a higher current peak. Therefore, for Mg-doped squared-like loops, the current peaks in the current density plots depicted in Figure 8 are higher and narrower than for the slanted P-E cycles of the undoped materials.

3.4 | High-power properties

As suggested by Bremecker et al.[9], the high stability of the NBT-BT-polycrystalline materials is due to the extremely high degree of poling-induced domain texture that minimizes the loss contribution arising from domain wall motion when specimens are tested in high-vibration mode. This high remanent texture, therefore, does not allow large extrinsic strain contributions from domain wall motion, leaving lattice extension as the main source of field-induced strain.

In Figure 9 and Figure S4, high-power coefficients as function of temperature of the NBT-6BT-0.5Mg

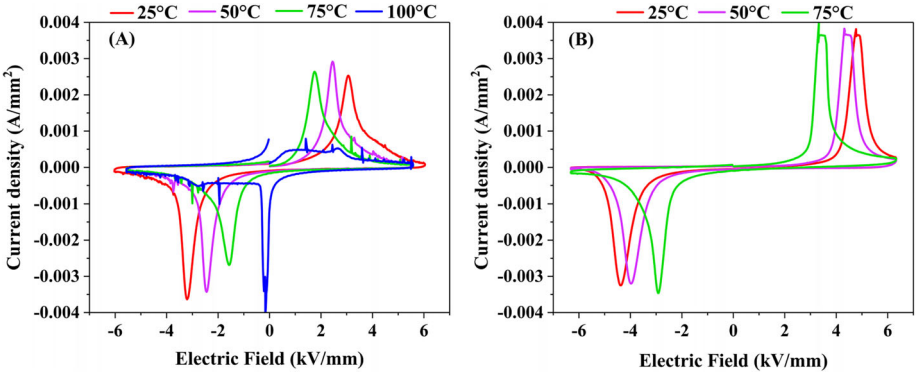

FIGURE 8 Current density versus electric field determined in the range of 25°C–100°C for NBT-6BT (A) and in the range of 25°C–75°C for NBT-6BT-0.5Mg (B) samples.

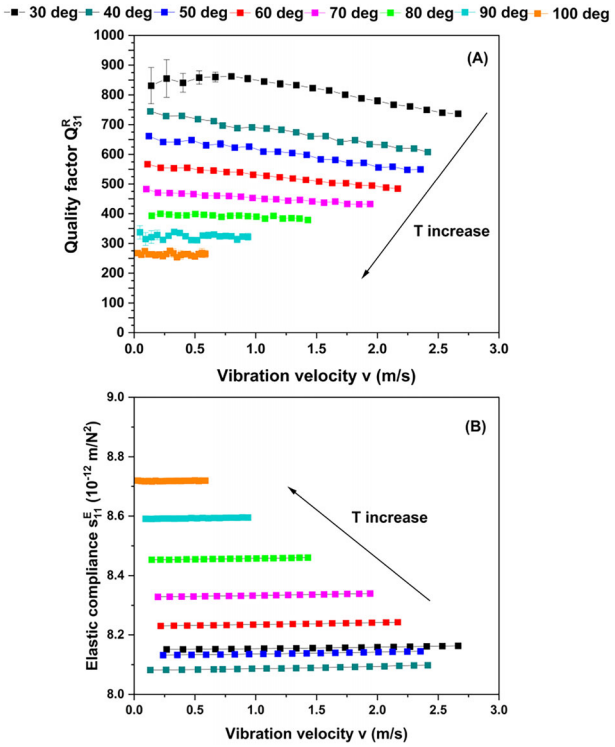

FIGURE 9 (A) Quality factor Q^R_{31} and (B) elastic compliance s^E_{11} of NBT-6BT-0.5Mg as function of vibration velocity and temperature.

system are depicted. Interested readers can find the trend of the same coefficients of the pure system in reference.[16]

High vibration velocity and stable quality factor have been reached in the doped system at 30°C (Figure 9A), which is four times larger than the undoped material one (Figure S3) consistent with Bremecker et al.[41]

The quality factor of the doped system decreased with temperature rise; however, it remains stable in the whole temperature range, and also at 70°C, which has been discovered to be a critical temperature for the doped material, the specimen reached a very high vibration velocity of 2 m/s.

Temperature has a strong effect on the elastic compliance of the material. As elastic compliance is the inverse of the stiffness of the material, the higher the elastic compliance, the less the material resists deformation in response to an applied force. The elastic compliance increases with increasing temperature (Figure 9B); in particular, an increase at 70°C could be noticed. In accordance with the rhombohedral to tetragonal phase transformation, the system becomes softer, and consequently, results in a lower stiffness. However, it is worth noting that despite the above-mentioned jump, the elastic compliance is independent on velocity at all investigated temperatures. As the density of the material can be assumed as constant in the measured temperature range, the elastic compliance is inversely proportional to the resonance frequency.[35] Thus, a stable elastic compliance implies working with a stable resonance frequency, which is desirable in high-power application.

4 | CONCLUSION

In this study, the temperature dependence of the poling-induced domain texture of NBT-6BT doped with 0.5 mol% Mg compared to undoped NBT-6BT was presented. The obtained degree of texture is close to the maximum achievable in both systems at room temperature. A critical temperature range between 70°C and 90°C has been identified where the textured rhombohedral structure transitions into an untextured tetragonal structure. This leads to anomalies found in thermally stimulated depolarization current and piezoelectric coefficient. Furthermore, the high-power measurements revealed strongly enhanced properties of the doped system as compared to the undoped one.

Therefore, poling-induced domain texturing is a viable approach capable of increasing the ferroelectric hardness of materials, although there may be limits to the temperature application.

ACKNOWLEDGMENTS

We are indebted to Wuzhen Laboratory for generous funding. Jurij Koruza is acknowledged for support with high-power measurements. Andreas Wohninsland would like to thank the Deutsche Forschungsgemeinschaft (DFG) for financial support under Nos. KO 5948/1-1 and KL 615/34-1 (grant number 414311761).

Open access funding enabled and organized by Projekt DEAL.

ORCID

Laura Cangini https://orcid.org/0009-0004-4346-0389
Daniel Bremecker https://orcid.org/0000-0002-8045-025X

REFERENCES

1. Wenk HR, Van Houtte P. Texture and anisotropy. Rep Prog Phys. 2004;67(8):1367–428. https://doi.org/10.1088/0034-4885/67/8/R02
2. Messing GL, Trolier-McKinstry S, Sabolsky EM, Duran C, Kwon S, Brahmaroutu B, et al. Templated grain growth of textured piezoelectric ceramics. Crit Rev Solid State Mater Sci. 2004;29(2):45–96.
3. Saito Y, Takao H, Tani T, Nonoyama T, Takatori K, Homma T, et al. Lead-free piezoceramics. Nature. 2004;432(7013):84–7. https://doi.org/10.1038/nature03028
4. Moriana AD, Zhang S. Lead-free textured piezoceramics using tape casting: a review. J Mater. 2018;4(4):277–303. https://doi.org/10.1016/j.jmat.2018.09.006
5. Jones JL. The use of diffraction in the characterization of piezoelectric materials. J Electroceramics. 2007;19(1):67–79. https://doi.org/10.1007/s10832-007-9048-z
6. Wan S, Bowman K. Modeling of electric field induced texture in lead zirconate titanate ceramics. J Mater Res. 2001;16(8):2306–13. https://doi.org/10.1557/JMR.2001.0317
7. Li JY, Rogan RC, Üstündag E, Bhattacharya K. Domain switching in polycrystalline ferroelectric ceramics. Nat Mater. 2005;4(10):776–81. https://doi.org/10.1038/nmat1485
8. Jones JL, Slamovich EB, Bowman KJ, Lupascu DC. Domain switching anisotropy in textured bismuth titanate ceramics. J Appl Phys. 2005;98(10):104102–104102-8. https://doi.org/10.1063/1.2128475
9. Bremecker D, Wohninsland A, Teuber S, Lalitha KV, Hinterstein M, Rödel J. Texture-based ferroelectric hardening in $Na_{1/2}Bi_{1/2}TiO_3$-based piezoceramics. Phys Rev Mater. 2023;7(4):10.1103/physrevmaterials.7.044603.
10. Carl K, Hardtl KH. Electrical after-effects in Pb(Ti, Zr)O_3 ceramics. Ferroelectrics. 1977;17(1):473–86. https://doi.org/10.1080/00150197808236770
11. Genenko YA, Glaum J, Hoffmann MJ, Albe K. Mechanisms of aging and fatigue in ferroelectrics. Mater Sci Eng B. 2015;192(C):52–82. https://doi.org/10.1016/j.mseb.2014.10.003
12. Rogan RC, Üstündag E, Clausen B, Daymond MR. Texture and strain analysis of the ferroelastic behavior of Pb(Zr, Ti)O_3 by in situ neutron diffraction. J Appl Phys. 2003;93(7):4104–11. https://doi.org/10.1063/1.1558229
13. Fan L, Zhang L, Ren Y, Liu H, Xing X, Chen J. Relationship among the crystal structure, texture, and macroscopic properties of tetragonal (Pb,La)(Zr,Ti)O_3 ferroelectrics investigated by in situ high-energy synchrotron diffraction. Inorg Chem. 2020;59(18):13632–8. https://doi.org/10.1021/acs.inorgchem.0c02002
14. Tutuncu G, Fan L, Chen J, Xing X, Jones JL. Extensive domain wall motion and deaging resistance in morphotropic 0.55Bi($Ni_{1/2}Ti_{1/2}$)O_3-0.45PbTiO_3 polycrystalline ferroelectrics. Appl Phys Lett. 2014;104:132907. https://doi.org/10.1063/1.4870506
15. Takenaka T. ($Bi_{1/2}Na_{1/2}$)TiO_3-$BaTiO_3$ system for lead-free piezoelectric ceramics. Jpn J Appl Phys. 1991;30:2236.
16. Slabki M, Lalitha KV, Rödel J, Koruza J. Origin of high-power drive stability in ($Na_{1/2}Bi_{1/2}$)TiO_3-$BaTiO_3$ based piezoceramics. Acta Mater. 2022;227:117703. https://doi.org/10.1016/j.actamat.2022.117703
17. Zhang S, Xia R, Lebrun L, Anderson D, Shrout TR. Piezoelectric materials for high power, high temperature applications. Mater Lett. 2005;59(27):3471–5. https://doi.org/10.1016/j.matlet.2005.06.016
18. Martin TSDG, Blumfield PICA. Piezoelectric materials for high temperature transducers and actuators. J Mater Sci Mater Electron. 2015;26(12):9256–67. https://doi.org/10.1007/s10854-015-3629-4
19. Rödel J, Webber KG, Dittmer R, Jo W, Kimura M, Damjanovic D. Transferring lead-free piezoelectric ceramics into application. J Eur Ceram Soc. 2015;35(6):1659–81. https://doi.org/10.1016/j.jeurceramsoc.2014.12.013
20. Koruza J, Bell AJ, Frömling T, Webber KG, Wang K, Rödel J. Requirements for the transfer of lead-free piezoceramics into application. J Mater. 2018;4(1):13–26. https://doi.org/10.1016/j.jmat.2018.02.001
21. Nguyen MD, Nazeer H. Vibration-level characteristics of lead-zirconate-titanate ceramics. Jpn J Appl Phys. 1992;31:3055.
22. Li T, Chen YH, Ma J. Frequency dependence of piezoelectric vibration velocity. Sensors Actuators, A. 2007;138(2):404–10. https://doi.org/10.1016/j.sna.2007.05.024
23. Liu G, Zhang S, Jiang W, Cao W. Losses in ferroelectric materials. Mater Sci Eng R Rep. 2015;89:1–48. https://doi.org/10.1016/j.mser.2015.01.002
24. Zheng J, Takahashi S, Yoshikawa S, Uchino K, de Vries JWC. Heat generation in multilayer piezoelectric actuators. J Am Ceram Soc. 1996;79(12):3193–8.
25. Priya S, Viehland D, Carazo AV, Ryu J, Uchino K. High-power resonant measurements of piezoelectric materials: Importance of elastic nonlinearities. J Appl Phys. 2001;90(3):1469–79. https://doi.org/10.1063/1.1381046
26. Uchino K. High-power piezoelectrics and loss mechanisms. In: Advanced piezoelectrics materials. Woodhead Publishing in Materials; 2017. p. 647–754.

27. Yan H, Reece MJ, Liu J, Shen Z, Kan Y, Wang P. Effect of texture on dielectric properties and thermal depoling of $Bi_4Ti_3O_{12}$ ferroelectric ceramics. J Appl Phys. 2006;100(7):10–3. https://doi.org/10.1063/1.2356092
28. Hollenstein E, Damjanovic D, Setter N. Temperature stability of the piezoelectric properties of Li-modified KNN ceramics. J Eur Ceram Soc. 2007;27(13–15):4093–7. https://doi.org/10.1016/j.jeurceramsoc.2007.02.100
29. Wu J, Xiao D, Wang Y, Wu W, Zhang B, Zhu J. Improved temperature stability of $CaTiO_3$-modified $[(K_{0.5}Na_{0.5})0.96Li_{0.04}](Nb_{0.91}Sb_{0.05}Ta_{0.04})O_3$ lead-free piezoelectric ceramics. J Appl Phys. 2008;104(2). https://doi.org/10.1063/1.2956390
30. Li L, Zhu M, Zhou K, Wei Q, Zheng M, Hou Y. Delayed thermal depolarization of $Bi_{0.5}Na_{0.5}TiO_3$-$BaTiO_3$ by doping acceptor Zn^{2+} with large ionic polarizability. J Appl Phys. 2017;122:204104. https://doi.org/10.1063/1.5012889
31. Das Adhikary G, Mahale B, Rao BN, Senyshyn A, Ranjan R. Depoling phenomena in $Na_{0.5}Bi_{0.5}TiO_3$-$BaTiO_3$: a structural perspective. Phys Rev B. 2021;103(18):15. https://doi.org/10.1103/PhysRevB.103.184106
32. Daniels JE, Jo W, Rödel J, Honkimäki V, Jones JL. Electric-field-induced phase-change behavior in $(Bi_{0.5}Na_{0.5})TiO_3$-$BaTiO_3$-$(K_{0.5}Na_{0.5})NbO_3$: a combinatorial investigation. Acta Mater. 2010;58(6):2103–11. https://doi.org/10.1016/j.actamat.2009.11.052
33. Esteves G, Ramos K, Fancher CM, Jones JL. LIPRAS: Line-Profile Analysis Software. 2017. DOI: 10.13140/RG.2.2.29970.25282/3
34. Jones JL, Slamovich EB, Bowman KJ. Domain texture distributions in tetragonal lead zirconate titanate by x-ray and neutron diffraction. J Appl Phys. 2005;97(3):034113–034113-6. https://doi.org/10.1063/1.1849821
35. Standard E. En 50324-2. Piezoelectric properties of ceramic materials and components - Part 2: Methods of measurement - low power. CLC; 2002.
36. Slabki M, Wu J, Weber M, Breckner P, Isaia D, Nakamura K, et al. Anisotropy of the high-power piezoelectric properties of $Pb(Zr,Ti)O_3$. J Am Ceram Soc. 2019;102(10):6008–17. https://doi.org/10.1111/jace.16464
37. Daniels JE, Jo W, Rödel J, Jones JL. Electric-field-induced phase transformation at a lead-free morphotropic phase boundary: case study in a 93% $(Bi_{0.5}Na_{0.5})$ TiO_3-7% $BaTiO_3$ piezoelectric ceramic. Appl Phys Lett. 2009;95(3):2007–10. https://doi.org/10.1063/1.3182679
38. Ma C, Guo H, Beckman SP, Tan X. Creation and destruction of morphotropic phase boundaries through electrical poling: a case study of lead-free $(Bi_{1/2}Na_{1/2})TiO_3$-$BaTiO_3$ piezoelectrics. Phys Rev Lett. 2012;109:107602. https://doi.org/10.1103/PhysRevLett.109.107602
39. Garg R, Rao BN, Senyshyn A, Krishna PSR, Ranjan R. Lead-free piezoelectric system $(Na_{0.5}Bi_{0.5})TiO_3$-$BaTiO_3$: equilibrium structures and irreversible structural transformations driven by electric field and mechanical impact. Phys Rev B. 2013;88:1014103. https://doi.org/10.1103/PhysRevB.88.014103
40. Wohninsland A, Fetzer AK, Broughton R, Jones JL, Lalitha KV. Structural and microstructural description of relaxor-ferroelectric transition in quenched $Na_{1/2}Bi_{1/2}TiO_3$-$BaTiO_3$. J Mater. 2022;8(4):823–32. https://doi.org/10.1016/j.jmat.2022.01.006
41. Bremecker D, Slabki M, Koruza J, Rödel J. Characterization of crystal structure, electrical and electromechanical properties of Mg-doped $0.94Na_{1/2}Bi_{1/2}TiO_3$-$0.06BaTiO_3$. J Eur Ceram Soc. 2022;42(13):5591–7.
42. Bremecker D, Lalitha KV, Teuber S, Koruza J, Rödel J. Influence of Zn^{2+} doping on the morphotropic phase boundary in lead-free piezoelectric 1-$Na_{1/2}Bi_{1/2}TiO_3$-x$BaTiO_3$. J Am Ceram Soc. 2022;105(2):1232–40. https://doi.org/10.1111/jace.18186
43. Ranjan R. $Na_{1/2}Bi_{1/2}TiO_3$-based lead-free piezoceramics: a review of structure-property correlation. Curr Sci. 2020;118(10):1507–19. https://doi.org/10.18520/cs/v118/i10/1507-1519
44. Xu C, Lin D, Kwok KW. Structure, electrical properties and depolarization temperature of $(Bi_{0.5}Na_{0.5})TiO_3$-$BaTiO_3$ lead-free piezoelectric ceramics. Solid State Sci. 2008;10(7):934–40. https://doi.org/10.1016/j.solidstatesciences.2007.11.003
45. Yoon MS, Lee YG, Ur SC. Effects of co-doped CaO/MnO on the piezoelectric/dielectric properties and phase transition of lead-Free $(Bi_{0.5}Na_{0.5})_{0.94}Ba_{0.06}TiO_3$ piezoelectric ceramics. J Electroceramics. 2009;23(2–4):564–71. https://doi.org/10.1007/s10832-008-9548-5
46. Anton EM, Jo W, Damjanovic D, Rdel J. Determination of depolarization temperature of $(Bi_{1/2}Na_{1/2})TiO_3$-based lead-free piezoceramics. J Appl Phys. 2011;110:094108. https://doi.org/10.1063/1.3660253
47. Slabki M, Venkataraman LK, Rojac T, Rödel J, Koruza J. Thermal stability of the electromechanical properties in acceptor-doped and composite-hardened $(Na_{1/2}Bi_{1/2})TiO_3$-$BaTiO_3$ ferroelectrics. J Appl Phys. 2021;130:014101. https://doi.org/10.1063/5.0052293
48. Schneider D, Rödel J, Rytz D, Granzow T. Orientation-dependence of thermal depolarization and phase development in $Bi_{1/2}Na_{1/2}TiO_3$-$BaTiO_3$ single crystals. J Am Ceram Soc. 2015;98(12):3966–74. https://doi.org/10.1111/jace.13843
49. Liu W, Randall CA. Thermally stimulated relaxation in Fe-doped $SrTiO_3$ systems: I. Single crystals. J Am Ceram Soc. 2008;91(10):3245–50. https://doi.org/10.1111/j.1551-2916.2008.02595.x
50. Yoon SH, Randall CA, Hur KH. Effect of acceptor (Mg) concentration on the resistance degradation behavior in acceptor (Mg)-doped $BaTiO_3$ bulk ceramics: I. Impedance analysis. J Am Ceram Soc. 2009;92(8):1758–65. https://doi.org/10.1111/j.1551-2916.2009.03121.x
51. Pugachev AM, Kovalevskii VI, Surovtsev NV, Kojima S, Prosandeev SA, Raevski IP, et al. Broken local symmetry in paraelectric $BaTiO_3$ proved by second harmonic generation. Phys Rev Lett. 2012;108:247601. https://doi.org/10.1103/PhysRevLett.108.247601
52. Aktas O, Salje EKH. Macroscopic symmetry breaking and piezoelectricity in relaxor ferroelectric lead magnesium niobate. Appl Phys Lett. 2018;113(20):202901. https://doi.org/10.1063/1.5055001
53. Jo W, Schaab S, Sapper E, Schmitt LA, Kleebe H-J, Bell AJ, et al. On the phase identity and its thermal evolution of lead free $(Bi_{1/2}Na_{1/2})TiO_3$-6 mol%$BaTiO_3$. J Appl Phys. 2011;110(7):074106. https://doi.org/10.1063/1.3645054
54. Iwamoto M. Maxwell–Wagner effect. In: Bhushan B, editor. Encyclopedia of nanotechnology. Dordrecht: Springer Netherlands; 2015. p. 1–13. https://doi.org/10.1007/978-94-007-6178-0_5-2
55. Koch L, Steiner S, Meyer KC, Seo IT, Albe K, Frömling T. Ionic conductivity of acceptor doped sodium bismuth titanate: Influence of dopants, phase transitions and defect associates. J Mater Chem C. 2017;5(35):8958–65. https://doi.org/10.1039/c7tc03031b

56. De Souza RA. Oxygen diffusion in $SrTiO_3$ and related perovskite oxides. Adv Funct Mater. 2015;25(40):6326–42. https://doi.org/10.1002/adfm.201500827

SUPPORTING INFORMATION

Additional supporting information can be found online in the Supporting Information section at the end of this article.

How to cite this article: Cangini L, Wohninsland A, Bremecker D, Fulanović L, Zhao C, Rödel J. Effect of thermal depolarization on the poling-induced domain texture and piezoelectric properties in Mg-doped NBT-6BT. J Am Ceram Soc. 2023;106:6879–6890. https://doi.org/10.1111/jace.19331